applied sciences

MDPI

Article

# Consensus Design for Heterogeneous Battery Energy Storage Systems with Droop Control Considering Geographical Factor

**Yalin Zhang [1], Yunzhong Song [1,*] and Shumin Fei [2]**

[1] School of Electrical Engineering and Automation, Henan Polytechnic University, Jiaozuo 454003, China; wrigley001@sina.com

[2] School of Automation, Southeast University, Nanjing 210096, China; smfei@seu.edu.cn

* Correspondence: songhpu@126.com; Tel.: +86-13839197011

Received: 7 January 2020; Accepted: 19 January 2020; Published: 20 January 2020


**Abstract:** This paper proposes a hierarchical control strategy to coordinate battery energy storage devices based on a multi-agent system. The heterogeneous nature of the battery volume is paid much more attention in designing the proportional protocol of the consensus controller. Besides that, a cluster algorithm based on Minimum Spanning Tree (MST) is suggested to represent geographical factor, and on account of that, each Battery Energy Storage System (BESS) is classified into its specific cluster zone. Further, an active leader is assigned to be in charge of information from the external side in every cluster. The consensus algorithm reconciles all clusters in a step-by-step way. Energy level, voltage, frequency and active/reactive power sharing of every BESS can reach consensus by an information exchange within and among clusters respectively. Further, a virtual leader is taken into the active leader role in directing frequency and voltage to the reference values. To verify the consensus algorithm, a modified IEEE 57-bus is employed for time-domain simulations in an islanded mode and all BESSs are working in a discharge model.

**Keywords:** Battery Energy Storage System (BESS); consensus; geographical factor; smart grid

## 1. Introduction

Energy storage technology is becoming the main method to stabilize the microgrid. A scheduling method for peak load shift of an energy storage system can increase power energy utilization rates and reduce economic expenditure of residents and power plants. Nowadays, more and more kinds of grid-connected renewable energy sources will contribute to the fluctuation of voltage and frequency, which can cause instability in the microgrid. An energy storage system can function as a power buffer and improve the quality of voltage and frequency. In other words, energy storage systems can be empowered as spare power sources when a fault appears in the grid [1–7].

Generally, the controller of energy storage is centralized or fully distributed. Compared with the centralized control, every energy storage only processes its relevant data in a distributed manner [8,9]. Therefore, distributed control has the characteristics of flexibility and reliability and is the common way in an energy storage system. In [10], distributed control is used to keep the balance between power output and load. To eliminate the attack of communication jamming, a distributed fuzzy logic-based control is adopted to ensure convergence under cyber-attack scenarios in [11].

A multi-agent system can cope with complex problems effectively in a power system and improve the robustness, reliability and flexibility of the system [12]. Therefore, lots of papers bring a multi-agent method into the controller of an energy storage system. For example, [13] introduces a multi-agent based distributed algorithm, by which the state-of-charge (SoC) of all energy storage units can reach

average consensus. In [14], a consensus algorithm based on a multi-agent system is proposed to solve the energy management problem.

In a single energy storage system, P/Q control and U/f control are the common methods, and the former carries out in a grid-connection mode while the latter puts into effect to retain the stability of voltage and frequency in island mode [15]. However, in the smart grid with multi storage systems, droop control is adopted to support load reliably [16,17] and propose a sparse communication network-based droop control to achieve power sharing, which can overcome the influence of output line impedances. Moreover, since microgrid does not have the characteristics of anti-interference capability, a PWM power converter of energy storage with droop control can operate in double quadrants, which can improve the inertia and damping of the grid. Thus, droop control can improve the capacity of resisting disturbance [18,19].

Challenges brings about power supply instability in the process of distributed generation integration into a power system, such as a voltage flicker [20]. Based on the above analysis, many researches focus on the performance of the storage incorporated into microgrid. [21] proposes the non-uniform droop gain ratio scheme to attain more accurate power sharing and restrain voltage and frequency fluctuation in the wind farm combined with the energy storage system. In [22], a flywheel merged into a wind farm can operate in an island model and support load to synchronize the system under the framework of a distributed algorithm. [23,24] proposed a distributed cooperative system and a secondary frequency controller for energy storages, whose power and energy level can reach a balance among the storages while the frequency can restore to the nominal value. In [25], the concept of heterogeneous nature of battery volume representing the capacity of power generation is drawn into a distributed controller to reach the power sharing consensus. Hierarchical control is applied to stabilize the frequency and voltage and restore the frequency and voltage to the nominal values by the secondary controller designed in [26]. Similarly, [27] designed a secondary voltage controller with feedback linearization to regulate the voltage of the distributed generation to the set values.

In fact, a large-scale power system is a common form in a large region, where the power generations can be distributed in a certain distance from each other. However, in all of the above existing studies, the location feature has not been considered. Therefore, inspired by [28] and in order to improve the cooperative control of the energy storage system [29], this paper designs a distributed step-by-step consensus algorithm based on droop controller considering geographical location. According to different geographical distributions, all BESSs can be divided into several clusters by the clustering algorithm based on Kruskal, which is a kind of MST algorithm [30]. The controller input can eliminate the gap of energy level, active power, voltage, frequency and reactive power among all BESSs. It is worth mentioning that the function of this consensus controller is similar to the primary controller. In addition, a virtual leader is built into the frequency and voltage inputs [31], which functioned as the secondary controller [32]. To be simplified, the hierarchical structure of the heterogeneous BESS model is compacted by the droop controller.

The left parts of the paper are arranged as follows. Section 2 presents the necessary preliminaries, which contains the Laplacian matrix and the clustering algorithm based on MST. The consensus algorithm is described in Section 3. IEEE 57-bus system is put use to test the proposed designs in Section 4. Finally, Section 5 is the summary of this paper.

## 2. Graph Theory

### 2.1. Improved Laplacian Matrix

In a multi-agent system, agents communicate with each other by an undirected connected graph $G(\Delta, \Gamma)$, which contains a vertex set $\Delta$ and an edge set $\Gamma$. In the edge set $\Gamma$, the weight $a_{ij}$ of edge $(i, j) \in \Gamma$ is equal to 0 or 1. That is, if agent $j$ is connected to $i$, $a_{ij} = 1$; if not, $a_{ij} = 0$. And the neighbor of agent $i$ is denoted by $N_i = \left\{ j : a_{ij} \neq 0 \right\}$. In addition, the degree matrix $D$ is a diagonal matrix and

expressed by $D = diag(d_i)_{i=1,\cdots,n}$, where $d_i = \sum_{j=1}^{n} a_{ij}$. Therefore, Laplacian matrix $L$ corresponding to $G$ is expressed as $L = D - A$, where $A = (a_{ij})_{n\times n}$ is the adjacency matrix of $G$.

Considering the location feature of each agent, an improved Laplacian matrix with the weight corresponding to each edge is adopted in this paper. In the edge set $\Gamma$, $a_{ij}$ is the reciprocal of relative distance between $i$ and $j$ in communication topology and implies the communication intensity of agent $i$ and $j$.

### 2.2. MST and Kruskal

In $G(\Delta, \Gamma)$, we can find one subgraph $g(\Delta, \boldsymbol{\varepsilon})$ which contains all vertexes and only a path from agent $i$ to agent $j$ for $\forall i, j \in \Delta$ and the sum of whose distances $w = \sum_{(i,j)\in\boldsymbol{\varepsilon}} 1/a_{ij}$ are the smallest, where $\boldsymbol{\varepsilon} \subset \Gamma$ and $g(\Delta, \boldsymbol{\varepsilon})$ is MST.

Kruskal is a kind of greedy algorithm based on union-find sets algorithm. It works out MST by traversing the edge as follows. Firstly, arrange all edges in ascending order. Secondly, traverse the shortest edge, processing it by union-find sets in turn. Finally, $g(\Delta, \boldsymbol{\varepsilon})$ contains $n$ vertexes and $n - 1$ edges.

### 2.3. A Clustering Algorithm Based on Kruskal

In this paper, BESSs are classified by clustering based on the Kruskal algorithm. Herein, $\boldsymbol{\varepsilon}_0$ is the set of all edges, and $\boldsymbol{\varepsilon}_k$ is the result of the algorithm in $k^{th}$ iteration, where one edge of $\boldsymbol{\varepsilon}_{k-1}$ is removed in order to get a new set $\boldsymbol{\varepsilon}_k$ under the condition that the objective function $\boldsymbol{\delta}_k$ in Equation (1) can get the maximum. When the inequality Equation (2) is satisfied, the iteration of the algorithm ends and this algorithm runs out.

$$\boldsymbol{\delta}_k = \left|\boldsymbol{\delta}(\boldsymbol{\varepsilon}_k) - \boldsymbol{\delta}(\boldsymbol{\varepsilon}_{k-1})\right| \tag{1}$$

$$\left|\boldsymbol{\delta}(\boldsymbol{\varepsilon}_k) - \boldsymbol{\delta}(\boldsymbol{\varepsilon}_{k-1})\right| < \left|\boldsymbol{\delta}(\boldsymbol{\varepsilon}_1) - \boldsymbol{\delta}(\boldsymbol{\varepsilon}_0)\right| \tag{2}$$

where $\boldsymbol{\delta}(\boldsymbol{\varepsilon}_k)$ is the variance of $\boldsymbol{\varepsilon}_k$. An isolated BESS will cause instability, especially when the load changes. It is reasonable that the isolated one is classified to the cluster of its nearest BESS, which belongs according to the location.

## 3. The Consensus Design

This paper proposes a step-by-step consensus algorithm with several active leaders or a virtual leader. In fact, active leaders are some agents while the virtual leader is an external command. All active leaders can reach consensus by exchanging information with each other and other agents can reach consensus according to their leader. The virtual leader can force all agents to follow the leader.

### 3.1. The Active Leader and the Virtual Leader

Figure 1 is a diagram of the step-by-step consensus controller. As shown in Figure 1, all agents are classified by the clustering algorithm in the last section, then select an agent as the leader in each cluster, i.e., L1 and L2. L1 in Cluster 1 and L2 in Cluster 2 are the active leaders in a), where they exchange information of their clusters with each other. L is the virtual leader in b), where L1 and L2 can receive the information from the leader. Accordingly, other agents in the set F1 and F2 will reach consensus under the guidance of their leader in each cluster. Every active leader in the cluster can play the role of active leader. For fast consensus, one can be select as active leader who has the largest number of neighbors. In order to save hardware/software, the virtual leader L should be incorporated into the active leader L1 and L2.

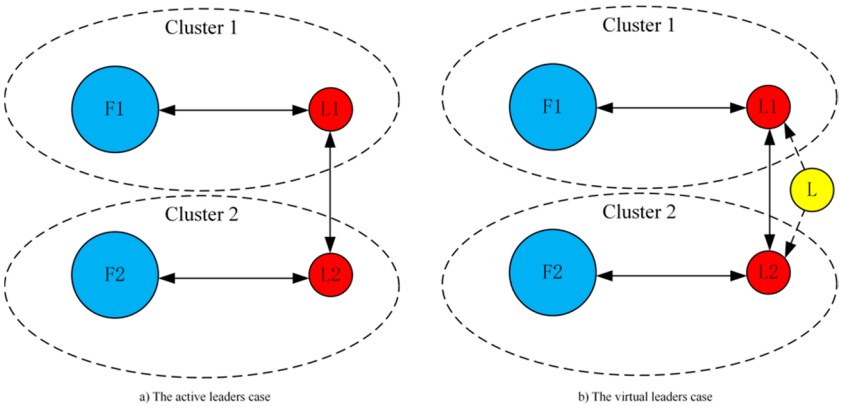


**Figure 1.** Example for the step-by-step consensus algorithm, L1 and L2 are active leaders, L is a virtual leader.

### *3.2. The Input Design of the Consensus for BESS*

Generally, the control structure of BESS shown in Figure 2 contains the inner current controller, the voltage controller, power calculation and droop controller [33–35]. However, the inner current controller and the voltage controller respond faster than the droop controller, and they can be ignored reasonably [36,37]. In other word, the control structure can be simplified by the droop controller expressed by Equation (3) which is used to maintain the stability of frequency and voltage in BESS.

$$\begin{bmatrix} \omega_i \\ V_i \end{bmatrix} = \begin{bmatrix} 1 & -1 & 0 & 0 \\ 0 & 0 & 1 & -1 \end{bmatrix} \begin{bmatrix} \omega_i^0 \\ K_i^P P_i \\ V_i^0 \\ K_i^Q Q_i \end{bmatrix} = \begin{bmatrix} 1 & -1 & 0 & 0 \\ 0 & 0 & 1 & -1 \end{bmatrix} \begin{bmatrix} \omega_i^0 \\ \widetilde{P}_i \\ V_i^0 \\ \widetilde{Q}_i \end{bmatrix} \tag{3}$$

where $\omega_i$ and $V_i$ are the frequency and voltage separately, $\omega_i^0$ and $V_i^0$ are the nominal frequency and the nominal voltage, $K_i^p$ and $K_i^Q$ are the droop gains. For simplicity, $K_i^P P_i$ and $K_i^P Q_i$ are denoted by $\widetilde{P}_i$ and $\widetilde{Q}_i$ in this paper. Similarly, [23] proposes a simplified model based on a droop controller for a large-scale energy system simulation. So, this paper designs a series of inputs of the simplified model to synchronize all BESSs, i.e., Equations (4) and (5).

$$\begin{bmatrix} \dot{\omega}_i^0 \\ \dot{\widetilde{P}}_i \\ \dot{E}_i \\ \dot{V}_i^0 \\ \dot{\widetilde{Q}}_i \end{bmatrix} = \begin{bmatrix} 0 & 0 & 0 & 0 & 0 \\ 0 & 0 & 0 & 0 & 0 \\ 0 & \frac{-1}{3600} & 0 & 0 & 0 \\ 0 & 0 & 0 & 0 & 0 \\ 0 & 0 & 0 & 0 & 0 \end{bmatrix} \begin{bmatrix} \omega_i^0 \\ \widetilde{P}_i \\ E_i \\ V_i^0 \\ \widetilde{Q}_i \end{bmatrix} + \begin{bmatrix} u_i^\omega \\ u_i^P \\ u_i^E \\ u_i^V \\ u_i^Q \end{bmatrix} \tag{4}$$

$$\begin{bmatrix} \omega_i \\ \widetilde{P}_i \\ E_i \\ V_i \\ \widetilde{Q}_i \end{bmatrix} = \begin{bmatrix} 1 & -1 & 0 & 0 & 0 \\ 0 & 1 & 0 & 0 & 0 \\ 0 & 0 & 1 & 0 & 0 \\ 0 & 0 & 0 & 1 & -1 \\ 0 & 0 & 0 & 0 & 1 \end{bmatrix} \begin{bmatrix} \omega_i^0 \\ \widetilde{P}_i \\ E_i \\ V_i^0 \\ \widetilde{Q}_i \end{bmatrix} \tag{5}$$

where $\omega_i$, $\widetilde{P}_i$, $E_i$, $V_i$ and $\widetilde{Q}_i$ are the frequency, active power, energy, voltage and reactive power of BESS respectively, $u_i^\omega$, $u_i^P$, $u_i^E$, $u_i^V$ and $u_i^Q$ are five inputs for BESS $i$, $\omega_i^0$ and $V_i^0$ are the nominal frequency and the nominal voltage of BESS $i$.

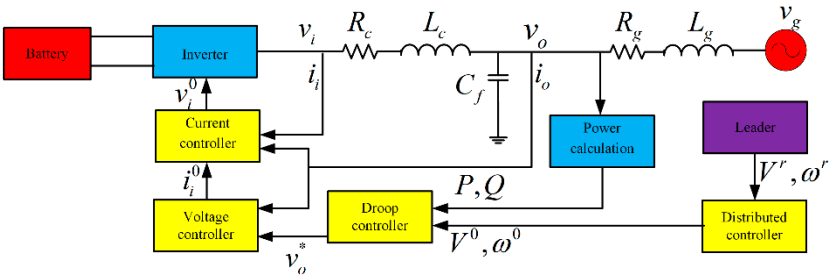


**Figure 2.** The hierarchical control structure of BESS.

### *3.3. The Design of the Input for Consensus*

This paper adopts the method of multi-agent to design the input presented in Equation (6).

$$\begin{bmatrix} u_i^{\omega} \\ u_i^{P} \\ u_i^{E} \\ u_i^{V} \\ u_i^{Q} \end{bmatrix} = \begin{bmatrix} -L_i\boldsymbol{\omega}^0 \\ -\frac{1}{K_i^P}L_i\widetilde{P} \\ -L_iE \\ -L_iV^0 \\ -\frac{1}{K_i^Q}L_i\widetilde{Q} \end{bmatrix} \tag{6}$$

where $L_i$ is the $i^{th}$ row of the Laplacian matrix $L$ corresponding to the topology $G$ of communication structure of BESSs, the column vector $\boldsymbol{\omega}^0$, $\widetilde{P}$, $E$, $V^0$ and $\widetilde{Q}$ are synthesis of the nominal frequency, active power, energy, the nominal voltage and reactive power of $n$ BESSs represented by $\boldsymbol{\omega}^0 = [\boldsymbol{\omega}_1^0, \cdots, \boldsymbol{\omega}_i^0, \cdots, \boldsymbol{\omega}_n^0]^T$, $\widetilde{P} = [\widetilde{P_1}, \cdots, \widetilde{P_i}, \cdots, \widetilde{P_n}]^T$, $E = [E_1, \cdots, E_i, \cdots, E_n]^T$, $V^0 = [V_1^0, \cdots, V_i^0, \cdots, V_n^0]^T$ and $\widetilde{Q} = [\widetilde{Q_1}, \cdots, \widetilde{Q_i}, \cdots, \widetilde{Q_n}]^T$, $1/K_i^P$ and $1/K_i^Q$ represent the ratio of active and reactive power and the capacity ratio of BESSs in [36].

### *3.4. The Design of the Input for Consensus with a Virtual Leader (Leader-Follower Consensus Algorithm)*

In order to realize the grid connection of BESS, frequency and voltage must restore to the nominal value of the grid. So, this paper introduces a virtual leader $\boldsymbol{0}(\boldsymbol{\omega}^r, V^r)$ incorporated into a BESS, which can lead frequency and voltage of all BESSs to $\boldsymbol{\omega}^r$ and $V^r$. Improved inputs are shown in Equations (7) and (8).

$$u_i^V = -L_iV^0 - a_{0i}(V_i^0 - \widetilde{Q}_i - V^r) \tag{7}$$

$$u_i^{\omega} = -L_i\boldsymbol{\omega}^0 - a_{0i}(\boldsymbol{\omega}_i^0 - \widetilde{P}_i - \boldsymbol{\omega}^r) \tag{8}$$

where $a_{0i}$ represents whether BESS $i$ is connected to the leader, i.e., in Equation (9).

$$a_{0i} = \begin{cases} 1, & i \subset N_0 \\ 0, & otherwise \end{cases} \tag{9}$$

### *3.5. The Design of the Input for Consensus*

It is assumed that $\boldsymbol{\tau}_{ij} > 0$ is the delay time on communication between from $j$ to $i$. In [38], a model with the communication delay in the topology of agents was proposed. Therefore, the same concept is introduced to this paper and the adjacency matrix is rewritten as Equation (10), which is applied to the step-by-step algorithm with the virtual leader.

$$A^{\tau}(i,j) = \begin{cases} 0, \ j = i \\ a_{ij}z^{-\boldsymbol{\tau}_{ij}}, j \in N_i \\ 0, \ otherwise \end{cases} \tag{10}$$

where $A^{\tau}(i,j)$ is the element in row $i$, column $j$, $z^{-\tau_{ij}}$ is the delay operator.

## 4. Case Study

### *4.1. The Design of the Input for Consensus*

In Figure 3, the weight of each edge represents relative distance between two BESSs and set the distance between BESS 2 and BESS 7 as 1. The result of the classification by the clustering algorithm is shown in Figure 3d. It shows that BESS 1,2,3,7 are in the same cluster while others are in the other cluster. To facilitate communication among the members of every cluster and between two clusters, BESS 7 and BESS 5 are selected as the active leader. The virtual leader is incorporated into BESS 7 and 5.

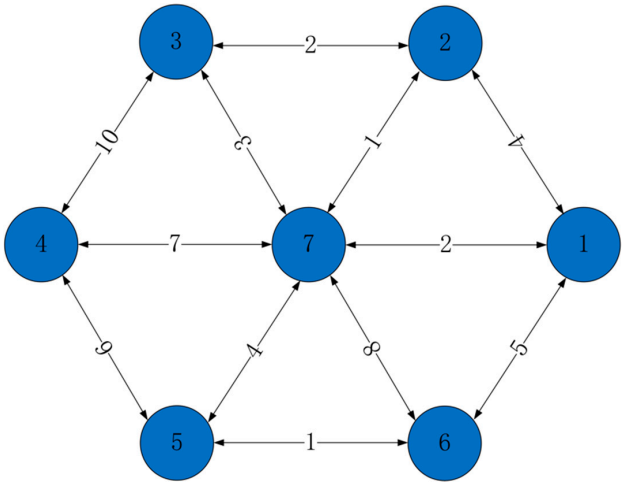


(a) The topology of communication of BESSs.

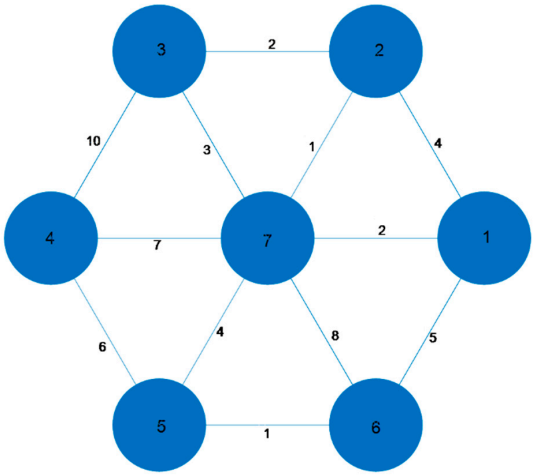


(b) The topology of communication of BESSs drawn by MATLAB.

**Figure 3.** *Cont.*

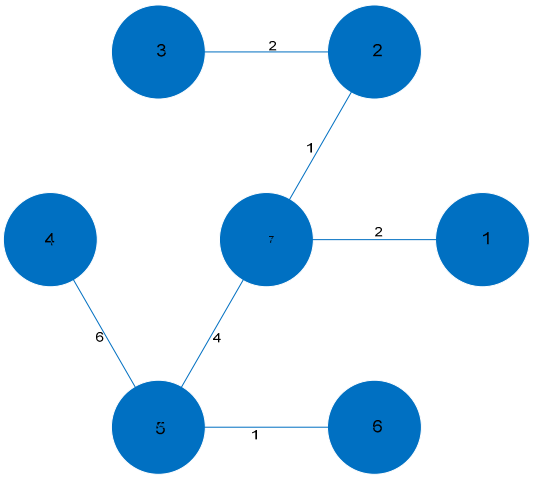


(c) The MST of (b).

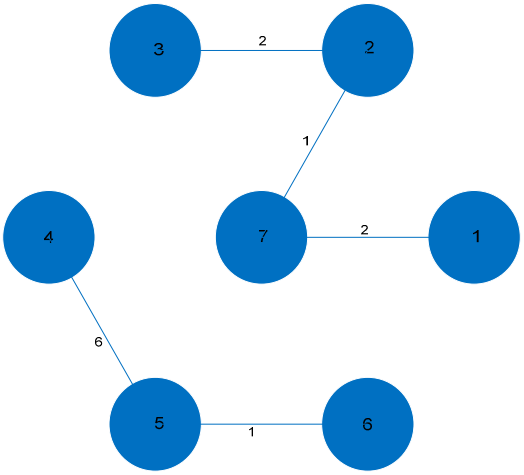


(d) The result of the performing clustering algorithm.

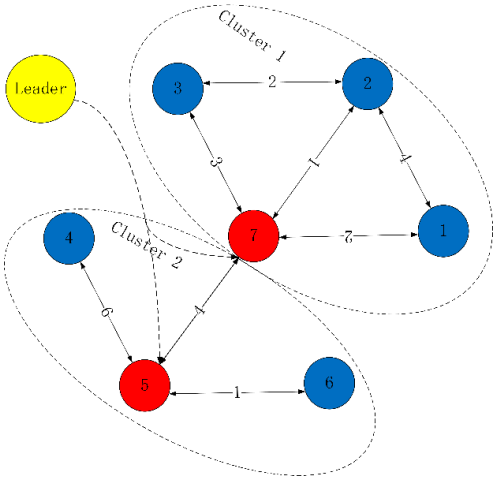


(e) The classification with a leader, BESS 7 is the leader of cluster 1 and BESS 5 is the leader of cluster 2.

**Figure 3.** Communication graph for test cases, (**a**) is the topology of communication of BESSs, (**b**) is drawn by MATLAB, (**c**) is the MST of (**b**), (**d**) is the result of performing clustering algorithm, (**e**) is the classification with a leader, BESS 7 is the leader of cluster 1 and BESS 5 is the leader of cluster 2.

### 4.2. Simulation Results

To verify the proposed algorithm, this paper adopts the IEEE 57-bus System as the test system [39]. The IEEE 57-bus System has seven generators and 42 load nodes shown in Figure 4. All generators are replaced by BESSs. According to [40–42], *MatDyn* is programmed for the dynamic simulation of synchronous generators, which is a toolbox based on the power flow calculation MATLAB Toolbox *MATPOWER*.

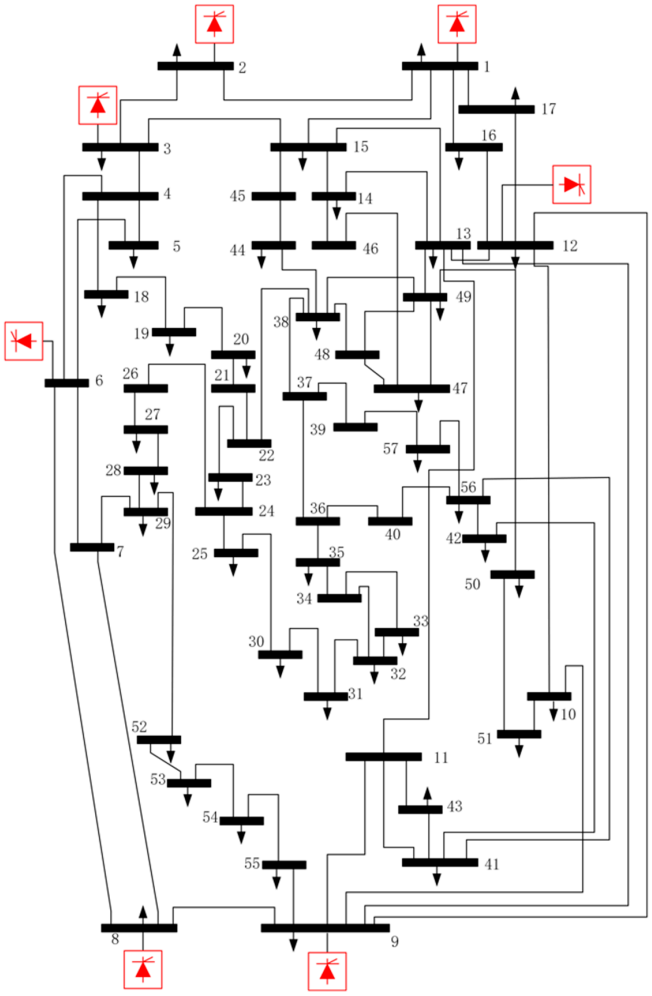


**Figure 4.** Modified IEEE 57-bus system.

To verify the proposed algorithm, this paper designs five cases in island mode and compares them with each other, where the specific values of droop gains are presented in Table 1.

**Table 1.** The parameters of consensus controller designed.

| Par. | Value | Par. | Value |
|---|---|---|---|
| $K_1^P$ | 1 | $K_1^Q$ | 1 |
| $K_2^P$ | 1.2 | $K_2^Q$ | 1.21 |
| $K_3^P$ | 1.25 | $K_3^Q$ | 1.3 |
| $K_4^P$ | 0.9 | $K_4^Q$ | 1.23 |
| $K_5^P$ | 0.95 | $K_5^Q$ | 0.95 |
| $K_6^P$ | 1.02 | $K_6^Q$ | 1.06 |
| $K_7^P$ | 1.1 | $K_7^Q$ | 1.13 |
| $\omega^r$ | $1p.u$ | $V^r$ | $1p.u$ |

#### 4.2.1. Case 1 Consensus Controller without Leader Regardless of Geographic Factors

This case is used to test the consensus algorithm without considering geographic factors proposed in this paper. The communication graph of BESSs is shown in Figure 3a, and the whole system is working in islanded mode. The consensus controller begins to work at 10 s. All BESSs will reach consensus at 12 s. In addition, there is a $1.26 + j1.26$ per unit ($p.u$) load decrease after 20 s and a $2.52 + j2.52 p.u$ load increase after 30 s. It is noteworthy that load changes are fully distributed among loads. As can be seen from Figure 5, whatever the load decreases or increases, active and reactive power sharing, frequency, voltage and energy level of all BESSs also can be synchronized and their final state can reach the average of their initial value. In addition, it can be observed that the consensus controller can act as the primary frequency/voltage controller.

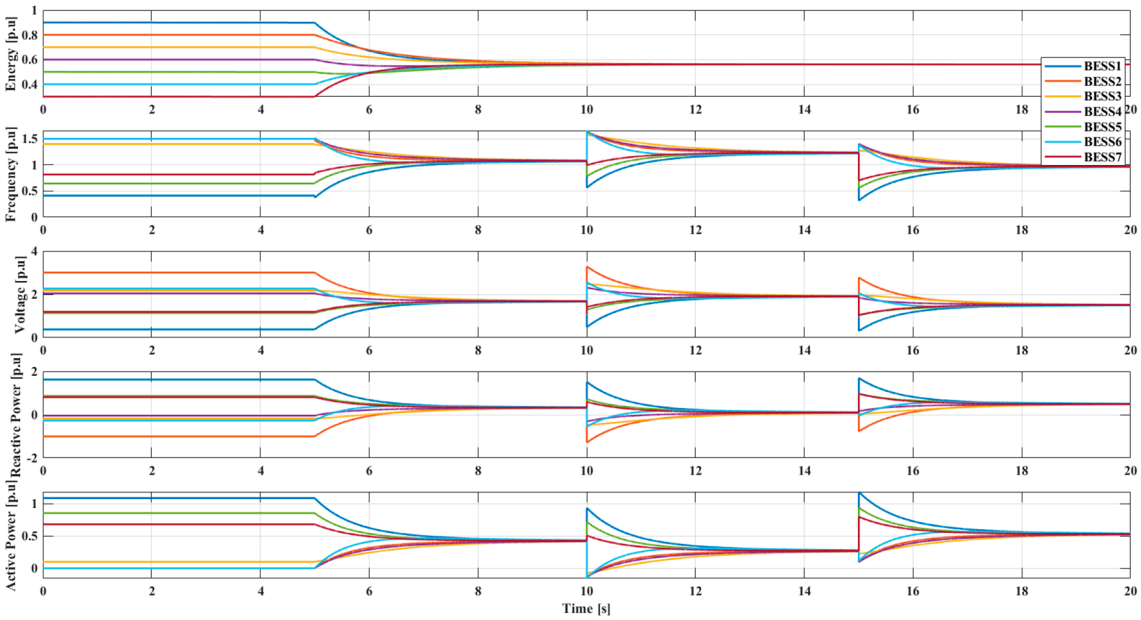


**Figure 5.** Simulation result without a leader regardless of geographic factors (case 1).

#### 4.2.2. Case 2 Consensus Controller without Leader Considering Geographic Factors

Under the same operating point change as in case 1, this case is used to test consensus controller considering the geographic factor without leaders. Similarly, all BESSs are working in an isolated model, and the communication topology of all BESSs is shown in Figure 3a. At the same time, a load decrement of $1.26 + j1.26 p.u$ and a load increment of $2.52 + j2.52 p.u$ at each load node occur at 20 s and 30 s respectively. Unlike case 1, the geographic factor is considered and the improved Laplacian matrix is applied in this case. It can be observed in Figure 6 that all BESSs reach consensus in this case slower than case 1, where BESS 4 is the slowest one. That is because there is a longer distance between BESS 4 and other BESSs, and every BESS reaches consensus at a different time according to the distance from its neighbor. Therefore, the convergence speed is affected by the geographic location.

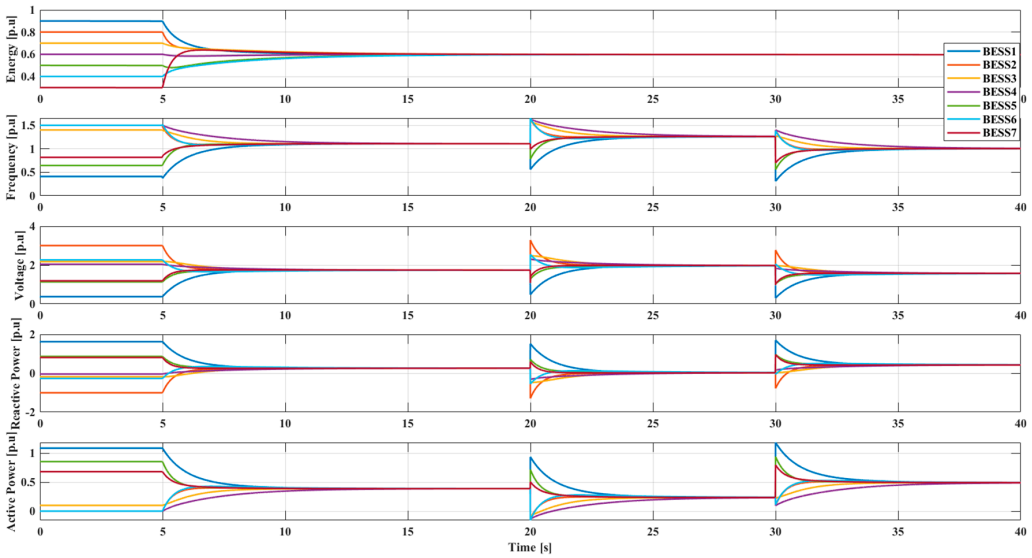


**Figure 6.** Simulation result without leader considering geographic factor (case 2).

#### 4.2.3. Case 3 Step-By-Step Case without the Virtual Leader

This case is used to test the effect of a step-by-step consensus algorithm considering geographic factors. The communication topology of all BESSs is shown in Figure 3e. The consensus controller is activated at 10 s. All BESSs in each cluster will reach consensus at 17 s, and then two clusters are coordinated. In addition, there is a $1.26 + j1.26p.u$ load decrease after 30 s and a $2.52 + j2.52p.u$ load increase after 50 s. It can be observed in Figure 7 that all BESSs can reach consensus in two steps. Firstly, BESS 1,2,3 and 7 in cluster 1 and BESS 4,5 and 6 in cluster 2 reach consensus respectively. Secondly, cluster 1 and cluster 2 reach consensus. Compared with case 1 and 2, the consensus speed is slower. It is noted that the speed of every BESS is negatively correlated with distance.

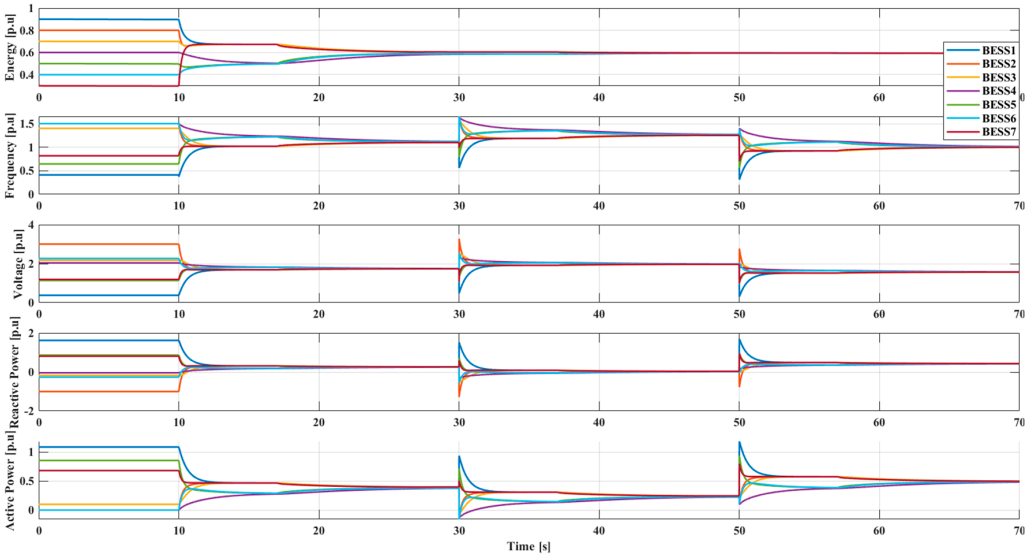


**Figure 7.** Simulation results of step-by-step consensus algorithm without the virtual leader (case 3).

#### 4.2.4. Step-By-Step Case with the Virtual Leader (Leader-Follower Consensus Algorithm)

This case is used to test the leader-follower consensus algorithm proposed in this paper. The communicate topology of all BESSs in Figure 3e is adopted. The consensus controller begins to work at five seconds. What is more, the same load change of each load node as the case 3 occurs at 50 s and 90 s. It is shown in Figure 8 that energy level, voltage, frequency, active power and reactive

power can reach consensus in two steps just as case 3. Furthermore, frequency and voltage restore to the nominal value 1 *p.u* whatever load changes. It can be observed that the leader-follower consensus controller can play a part of the secondary frequency/voltage controller.

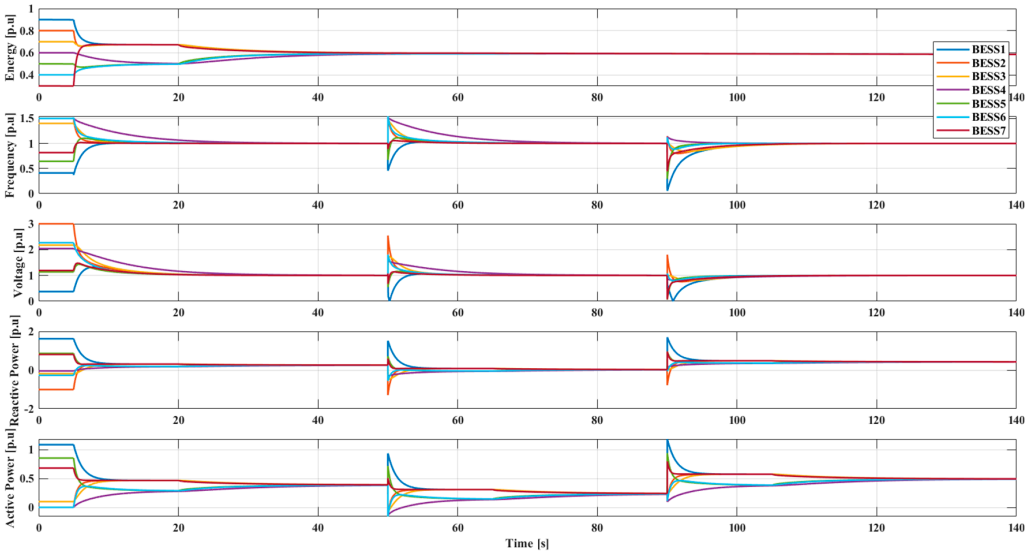


**Figure 8.** Simulation results of step-by-step consensus algorithm with the virtual leader (case 4).

#### 4.2.5. The Effect of Communication Delay

This case is used to cope with the delay of the communication topology proposed under the same operating point change in case 4. All BESSs communicate with each other over a topology structure shown in Figure 3e. Besides, the load change is the same as in case 4. To facilitate grid connection, the reference values of voltage and frequency in the virtual leader are set as 1 *p.u*. The delay time is set as 100 ms and is far beyond the upper limit, which is defined as 16 ms by the IEEE and international electro-technical commission (IEC) to ensure the stability of the grid [43]. As shown in Figure 9, although communication delay causes some oscillations and a longer time to reach consensus, energy level, voltage, frequency and active/reactive power all can be synchronized. Besides, voltage and frequency can be regulated to 1 *p.u*, which are the most important conditions for the grid connection of the microgrid.

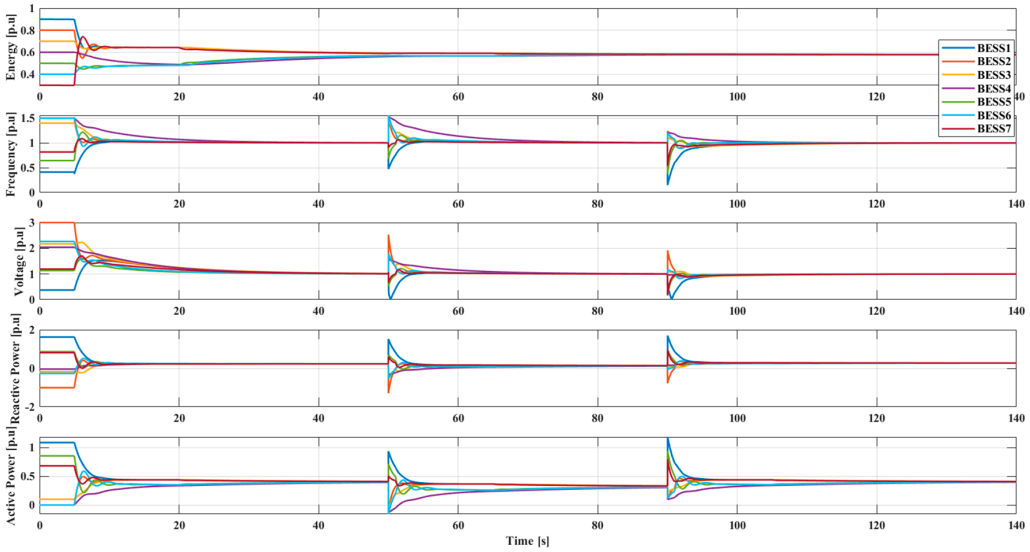


**Figure 9.** Simulation results of the consensus algorithm with communication delay (case 5).

## 5. Conclusions

This paper proposes a distributed control method to coordinate multi BESSs in a microgrid working in an island model. Based on a geographical factor, a cluster algorithm based on MST proposed is used to classify BESS. Meanwhile, a simplified model of heterogeneous BESS with a secondary droop controller is applied in this paper. Furthermore, the step-by-step consensus algorithm based on a geographical factor is put into effect to realize the balance of the active/reactive power sharing, energy level, voltage, frequency among all BESSs. To facilitate the grid connection of BESSs, the reference incorporated into the active leader can lead to the reference value of voltage and frequency. Compared with the average consensus algorithm regardless of a geographical factor, the consensus algorithm proposed can realize not only the synchronization of BESSs, but also that the synchronization speed varies depending on location. It remains stable and synchronizes when the system meets the communication delay.

**Author Contributions:** Conceptualization, Y.S. and S.F.; methodology, Y.S.; validation, Y.Z.; formal analysis, Y.S., S.F. and Y.Z.; writing—original draft preparation, Y.Z.; writing—review and editing, S.F. All authors have read and agreed to the published version of the manuscript.

**Funding:** This research was funded by the Natural Science Foundation of Henan Province, grant number 182300410112, and by the National Natural Science Foundation of China, grant number 61340041, 61374079 and 61903126.

**Acknowledgments:** The authors would like to thank the Natural Science Foundation of Henan Province (182300410112) and the National Natural Science Foundation of China (61340041, 61374079, 61903126).

**Conflicts of Interest:** The authors declare no conflict of interest.

## Nomenclature

| | |
|---|---|
| $i$, $N_i$ | Index of BESSs and the neighbor set of BESS $i$ |
| $G$, $D$ | The topology of communication and its degree matrix |
| $L$, $A$ | Laplacian matrix and adjacency matrix of the communication graph |
| $a_{ij}$ | The $(i, j)$-th element of $A$ |
| $g$ | The topology of MST |
| $\widetilde{P}_i$, $\widetilde{Q}_i$, $\boldsymbol{\omega}_i$, $V_i$, $E_i$ | The active/reactive power, frequency, voltage and energy level of BESS $i$ |
| $\boldsymbol{\omega}_i^0$, $V_i^0$ | The rated frequency and voltage of BESS $i$ |
| $V^r$, $\boldsymbol{\omega}^r$ | The reference frequency and voltage |
| $u_i^{\omega}$, $u_i^P$, $u_i^E$, $u_i^V$, $u_i^Q$ | The designed input of BESS $i$ |
| $K_i^P$, $K_i^Q$ | The coefficient of droop controller for BESS $i$ |
| $\boldsymbol{\tau}_{ij}$ | The delay time from BESS $j$ to $i$ |
| $A^{\boldsymbol{\tau}}$ | The adjacency matrix of the communication graph with delay time |

## References

1. Tushar, W.; Chai, B.; Yuen, C.; Huang, S.; Smith, D.B.; Poor, H.V.; Yang, Z. Energy storage sharing in smart grid: A modified auction-based approach. *IEEE Trans. Smart Grid* **2014**, *7*, 1462–1475.
2. Guobin, X.; Wei, Y.; David, G.; Nada, G.; Paul, M. Toward integrating distributed energy resources and storage devices in smart grid. *IEEE Internet Things J.* **2017**, *4*, 192–204.
3. Hung, K.N.; Ju, B.S.; Zhu, H. Distributed Demand side management with energy storage in smart grid. *IEEE Trans. Parallel Distrib. Syst.* **2015**, *26*, 3346–3357.
4. Chiang, S.J.; Chang, K.T.; Yen, C.Y. Residential photovoltaic energy storage system. *IEEE Trans. Ind. Electron.* **2015**, *26*, 3346–3357. [CrossRef]
5. Xiangjun, L.; Dong, H.; Xiaokang, L. Battery energy storage station (BESS)-based smoothing control of photovoltaic (PV) and wind power generation fluctuations. *IEEE Trans. Sustain. Energy* **2013**, *4*, 464–473.
6. Hill, C.A.; Such, M.C.; Chen, D.; Gonzalez, J.; Grady, W.M. Battery energy storage for enabling integration of distributed solar power generation. *IEEE Trans. Smart Grid* **2012**, *3*, 850–857. [CrossRef]
7. Wang, X.; Liu, Y. Analysis of energy storage technology and their application for micro grid, 2017. In Proceedings of the International Conference on Computer Technology, Electronics and Communication (ICCTEC), Sanya, China, 25–26 June 2017.

8. Karl, W.; Christopher, M.K.; Philipp, B.; Lars, G.; Steven, R.W. Distributed and decentralized control of residential energy systems incorporating battery storage. *IEEE Trans. Smart Grid* **2015**, *6*, 1914–1923.
9. Sriram, G.; Anand, S.; Bhuvan, U. Benefits and limitations of tapping into stored energy for datacenters. In Proceedings of the 38th International Symposium on Computer Architecture (ISCA 2011), San Jose, CA, USA, 4–8 June 2011.
10. Yinliang, X.; Wei, Z.; Gabriela, H.; Soummya, K.; Zhicheng, L. Cooperative control of distributed energy storage systems in a Microgrid. *IEEE Trans. Smart Grid* **2015**, *6*, 238–248.
11. Desh, D.S.; Singh, S.N.; Jeremy, L.; Elham, F. Agent-based distributed control schemes for distributed energy storage systems under cyber attacks. *IEEE J. Emerg. Sel. Top. Circuits Syst.* **2017**, *7*, 307–318.
12. Aris, L.D.; Nikos, D.H. Operation of a multiagent system for microgrid control. *IEEE Trans. Power Syst.* **2005**, *20*, 1447–1455.
13. Chendan, L.; Ernane, A.A.C.; Tomislav, D.; Josep, M.G.; Juan, C.V. Multiagent-based distributed state of charge balancing control for distributed energy storage units in AC microgrids. *IEEE Trans. Ind. Appl.* **2017**, *53*, 2369–2381.
14. Chengcheng, Z.; Jianping, H.; Jiming, C. Consensus-based energy management in smart grid with transmission losses and directed communication. *IEEE Trans. Smart Grid* **2017**, *8*, 2049–2061.
15. Lu, X.; Sun, K.; Guerrero, J.M.; Quintero, J.C.V.; Huang, L.; Teodorescu, R. SoC-based droop method for distributed energy storage in DC microgrid applications. *IEEE Int. Symp. Ind. Electron.* **2012**, *6*, 1640–1645.
16. Xiaonan, L.; Kai, S.; Josep, M.G.; Juan, C.V.; Lipei, H. State-of-charge balance using adaptive droop control for distributed energy storage systems in DC microgrid applications. *IEEE Trans. Ind. Electron.* **2014**, *61*, 2804–2815.
17. Lin-Yu, L.; Chia-Chi, C. Consensus-based droop control synthesis for multiple DICs in isolated microgrids. *IEEE Trans. Power Syst.* **2015**, *30*, 2243–2256.
18. Lin-Yu, L.; Chia-Chi, C. Consensus-based droop control of isolated micro-grids by ADMM implementations. *IEEE Trans. Smart Grid* **2018**, *9*, 5101–5112.
19. Xiaonan, L.; Kai, S.; Josep, M.G.; Juan, C.V.; Lipei, H. Double-quadrant state-of-charge-based droop control method for distributed energy storage systems in autonomous DC microgrids. *IEEE Trans. Smart Grid* **2015**, *6*, 147–157.
20. Nelson, F.A.; Chia-Chi, C. Distributed pinning droop control in isolated AC microgrids. *IEEE Trans. Ind. Appl.* **2017**, *53*, 3237–3249.
21. Lin-Yu, L.; Chia-Chi, C. Consensus-based P-f/Q-V droop control in autonomous micro-grids with wind generators and energy storage systems. In Proceedings of the IEEE PES General Meeting Conference & Exposition, National Harbor, MD, USA, 27–31 July 2014; pp. 1–5.
22. Qian, C.; Yong-Duan, S.; Josep, M.; Shulin, T. Coordinated control for flywheel energy storage matrix systems for wind farm based on charging/discharging ratio consensus algorithms. *IEEE Trans. Smart Grid* **2016**, *7*, 1259–1267.
23. He, C.; Guoqiang, H. Consensus-based distributed package-level state-of-charge balancing for grid-connected battery energy storage system. In Proceedings of the 12th IEEE International Conference on Control & Automation (ICCA), Kathmandu, Nepal, 1–3 June 2016.
24. Thomas, M.; Branislav, H.; Vassilios, G.A. Distributed cooperative control of microgrid storage. *IEEE Trans. Power Syst.* **2015**, *30*, 2780–2789.
25. Thomas, M.; Branislav, H.; Vassilios, G.A. Cooperative multi-agent control of heterogeneous storage devices distributed in a DC microgrid. *IEEE Trans. Power Syst.* **2016**, *31*, 2974–2986.
26. Josep, M.G.; Juan, C.V.; José, M.; Luis, G.V.; Miguel, C. Hierarchical control of droop-controlled AC and DC microgrids—A general approach toward standardization. *IEEE Trans. Ind. Electron.* **2011**, *58*, 158–172.
27. Ali, B.; Ali, D.; Frank, L.L.; Josep, M.G. Distributed cooperative secondary control of microgrids using feedback linearization. *IEEE Trans. Power Syst.* **2013**, *28*, 3462–3470.
28. Dinh, H.N. A sub-optimal consensus design for multi-agent systems based on hierarchical LQR. *Automatica* **2015**, *55*, 88–94.
29. Reza, O.S.; Alex, F.; Richard, M.M. Consensus and cooperation in networked multi-agent systems. *Proc. IEEE* **2007**, *95*, 215–233. [CrossRef]
30. Xiao-bo, L.; Ma, C.Y. A Clustering algorithm based on minimum spanning tree and cluster centers. *Math. Probl. Eng.* **2018**, *5*, 1–14.

31. Dinh, H.N.; Tatsuo, N.; Michihiro, K. Output consensus design for heterogeneous nonlinear multi-agent systems with application to smart grids. In Proceedings of the 2015 IEEE 54th Annual Conference on Decision and Control (CDC), Osaka, Japan, 15–18 December 2015.
32. Fanghong, G.; Changyun, W.; Jianfeng, M.; Yong-Duan, S. Distributed secondary voltage and frequency restoration control of droop-controlled inverter-based microgrids. *IEEE Trans. Ind. Electron.* **2015**, *62*, 4355–4364.
33. Amit, J.; Karan, J.; Aman, B.; Ned, M. Voltage regulation with STATCOMs: Modeling, control and results. *IEEE Trans. Power Deliv.* **2006**, *21*, 726–735.
34. Lennart, H.; Massimo, B.; Stefan, L. Input-admittance calculation and shaping for controlled voltage-source converters. *IEEE Trans. Ind. Electron.* **2007**, *54*, 3323–3334.
35. Nagaraju, P.; Milan, P.; Timothy, C.G. Modeling, Analysis and testing of autonomous operation of an inverter-based microgrid. *IEEE Trans. Power Electron.* **2007**, *22*, 613–625.
36. Javad, K.; Dinh, H.N. Multi-agent consensus design for heterogeneous energy storage devices with droop control in smart grids. *IEEE Trans. Smart Grid* **2019**, *10*, 1395–1404.
37. Javad, K.; Zhixin, M. Consensus control for energy storage system. *IEEE Trans. Smart Grid* **2018**, *9*, 3009–3017.
38. Morstyn, T.; Hredzak, B.; Agelidis, V.G. Communication delay robustness for multi-agent state of charge balancing between distributed AC microgrid storage systems. In Proceedings of the IEEE Conference Control Applications, Sydney, NSW, Australia, 21–23 September 2015; pp. 181–186.
39. Power Systems and Evolutionary Algorithms. Available online: https://al-roomi.org/ (accessed on 17 May 2015).
40. Cole, S.; Belmans, R. MatDyn, A New Matlab-Based Toolbox for Power System Dynamic Simulation. *IEEE Trans. Power Syst.* **2011**, *26*, 1129–1136. [CrossRef]
41. MatDyn—Electa. Available online: https://www.esat.kuleuven.be/electa (accessed on 4 February 2010).
42. Matpower-Free, Open-Source Tools for Electric Power System Simulation and Optimization. Available online: https://matpower.org/ (accessed on 20 July 2019).
43. Gungor, V.C.; Sahin, D.; Kocak, T.; Ergut, S.; Buccella, C.; Cecati, C.; Hancke, G.P. A survey on smart grid potential applications and communication requirements. *IEEE Trans. Ind. Inf.* **2013**, *9*, 28–42. [CrossRef]